*sustainability*

MDPI

*Article*

# Enhancing the Efficiency of Photovoltaic Power Flows Management in Three-Phase Prosumer Grids

**Laurynas Šriupša [1,*], Mindaugas Vaitkūnas [1,2], Artūras Baronas [1], Gytis Svinkūnas [1], Julius Dosinas [1], Andrius Knyš [1], Saulius Gudžius [1], Audrius Jonaitis [1] and Darius Serva [1]**

[1] Department of Electrical and Energy Systems, Kaunas University of Technology, Studentu Str. 48, LT-51367 Kaunas, Lithuania; mindaugas.vaitkunas@ktu.lt (M.V.); arturas.baronas@ktu.lt (A.B.); gytis.svinkunas@ktu.lt (G.S.); julius.dosinas@ktu.lt (J.D.); andrius.knys@ktu.lt (A.K.); saulius.gudzius@ktu.lt (S.G.); audrius.jonaitis@ktu.lt (A.J.); darius.serva@ktu.edu (D.S.)

[2] Faculty of Informatics, Engineering and Technologies, Kauno Kolegija Higher Education Institution, Pramones Av. 20, LT-50468 Kaunas, Lithuania

* Correspondence: laurynas.sriupsa@ktu.edu; Tel.: +370-64016124

**Abstract:** Households with photovoltaic installations contribute to reducing greenhouse gas emissions and mitigating global climate change. To fully utilize the benefits of clean solar energy, it is essential to ensure its efficient use, which can be achieved by consuming all generated energy locally, within the household or a microgrid community, eliminating wastage during the grid transportation and storage. In this work, we propose a method to enhance self-consumption by eliminating simultaneous bidirectional energy flow in the phase lines of a three-phase grid-tied household system, particularly in cases of significant load asymmetry. We developed an adaptive power flow management (APFM) algorithm which distributes solar-generated energy across the household grid's phase lines based on their respective loads and solar power generation level. A simulation based on real-world data demonstrated that the APFM algorithm both eliminates simultaneous active power import and export flows and ensures that all power exported from the household to the DSO grid remains symmetrical across all phase lines. As observed from the simulation results, applying the APFM algorithm reduced the daily imported and exported energy between the household and the DSO grid by an average of 27.5% during the spring–autumn period for a specific household. Additionally, reducing energy flow led to a 5% average increase in self-consumption within the household grid, with peak improvements reaching 16.5%.

**Keywords:** photovoltaic; inverter control algorithm; three-phase prosumer grid; asymmetric phase line loads; self-consumption; adaptive power flow management; bidirectional power flow



Academic Editor: Jiageng Ruan

Received: 30 January 2025
Revised: 24 February 2025
Accepted: 26 February 2025
Published: 1 March 2025

**Citation:** Šriupša, L.; Vaitkūnas, M.; Baronas, A.; Svinkūnas, G.; Dosinas, J.; Knyš, A.; Gudžius, S.; Jonaitis, A.; Serva, D. Enhancing the Efficiency of Photovoltaic Power Flows Management in Three-Phase Prosumer Grids. *Sustainability* **2025**, *17*, 2134. https://doi.org/10.3390/su17052134



## 1. Introduction

The European Green Deal initiative, introduced by the European Commission, aims to accelerate the adoption of renewable energy and promote efficient energy use to achieve climate neutrality by 2050. Energy efficiency, including electricity, is essential for both environmental sustainability and economic growth. Households in Lithuania and other EU countries play a vital role in expanding renewable electricity adoption and have significant potential to improve energy consumption efficiency in the future. Smarter and more efficient management of self-generated energy supports sustainable development, leading to both lower electricity costs and a substantial reduction in carbon footprint.

Over the past decade, the breakthrough in adoption of photovoltaic (PV) installations has mainly been driven by three key factors: advances in technology, costs reduction, and

support policies implemented by governments. However, the rapid expansion of solar power plants also brings new challenges for both grid operators and consumers themselves. The inherent variability of photovoltaic electricity generation, driven by fluctuating solar irradiation, becomes more problematic as the installed capacity of solar plants grows. This expansion increases grid instability, resulting in more frequent voltage fluctuations, frequency deviations, current and voltage harmonics, and a widening imbalance between supply and demand [1–6]. It is also important to note that most household devices are single-phase, which contributes to uneven load distribution across phase lines and causes voltage imbalances in the network. The problem becomes even more obvious as more small single-phase solar power plants are connected to the DSO grid [7–11]. Ultimately, this creates a barrier to further expansion of individual renewable generation capacity [5,9,12–14].

One of the most effective solutions to address generation imbalance issues is the use of high-capacity energy storage systems (ESSs) to store excess energy [11,15]. Energy storage systems help balance the mismatch between renewable electricity generation and daytime consumption. They also reduce load imbalances in the distribution grid when operating in on-grid mode [16–19]. However, the high costs of many types of ESSs and their relatively fast degradation mean that initial investments are often not cost-effective [20,21]. These factors largely explain why ESS adoption remains limited.

An alternative approach involves adjusting the individual energy consumption model by encouraging the use of energy-intensive devices during peak daylight hours [22,23]. Although it is technically straightforward and does not rely on energy storage, this approach nonetheless requires behavioral changes from consumers, which can impact comfort and quality of life, making it less appealing to many users today.

One more solution, that effectively addresses the supply and demand imbalance and increases self-consumption of locally generated electricity, is the establishment of consumer communities, where multiple neighboring consumers are integrated into a single large-scale microgrid. In these communities, one or more photovoltaic sources supply energy that is distributed among all members, resulting in greater local consumption of generated energy [24–26]. While the idea seems appealing in theory, there are not many practical examples of such implementations. Establishment and maintenance of such consumer community microgrids requires substantial infra-structure investment and creation of an appropriate regulatory framework in each country. Considering the current situation, rapid widespread adoption of community microgrids is unlikely in the near future.

A solar inverter with a certain load-sensitive control algorithm implemented into the prosumer's household grid can be another possible solution to eliminate the imbalance of the three-phase grid and improve the grid quality parameters [6,11,27]. For instance, one study [28] de*SCR*ibes an inverter control method that adjusts voltage magnitude and addresses voltage unbalance through reactive power injections into the distribution grid. The simulation results demonstrate the relation of reactive power at the inverter output to grid voltage imbalance and power losses. Another study [29] presents a dual-mode inverter—both grid-following and grid-forming—with a hierarchical control structure which incorporates power, voltage, and current control loops. This system can regulate grid voltage and limit current under unbalanced conditions. Yet another study [30] introduces a control algorithm for a the three-phase four-wire inverter, which follows load currents of three-phase grid lines to compensate the unbalance between those lines. The research is based on the computer simulation of the DSO grid segment which includes real-world data. The proposed control algorithm improves the symmetry of phase lines' voltages and maintains permissible voltage ranges. However, most of these studies lack a detailed examination of real-life daily power flows between three-phase prosumers and the DSO grid under unbalanced conditions, as well as a thorough quantitative assessment of the

prosumer losses caused by this imbalance. One study [31] analyzes the asymmetric loading of phases in a household grid and proposes a compensation mechanism based on evaluating average power flows in 10 min time intervals. However, this methodology is unsuitable for accurately balancing power flows in a household microgrid, as photovoltaic (PV) generation and household loads can fluctuate multiple times within a 10 min interval. Furthermore, both Muiste et al. [31] and our previous research [32] highlight the inefficient utilization of PV-generated electricity, where energy is exported to the DSO grid by one phase line and simultaneously imported to the household grid by another. These factors served as the primary motivation for developing a more precise and efficient power flow management approach for three-phase prosumer grids.

This paper further examines the challenges caused by load imbalance in individual prosumer systems and explores a potential solar inverter control algorithm. The proposed approach aims to fully mitigate simultaneous bidirectional power flows caused by load imbalances across phase lines in a prosumer's household microgrid. A load-adaptive photovoltaic power redistribution strategy for three-phase microgrids is introduced, along with the development of an adaptive power flow management (APFM) algorithm. The novelty of the proposed algorithm and methodology lies in its ability to evaluate and balance power flow changes within phase lines of the microgrid at one-second intervals, ensuring more accurate and dynamic control.

## 2. Simultaneous Bidirectional Power Flows

Individual prosumers with solar power systems encounter additional challenges rarely discussed in the literature. These include managing photovoltaic power flows in an unbalanced three-phase household grid. A typical structure of a grid-connected household system with its own solar plant is presented in Figure 1.

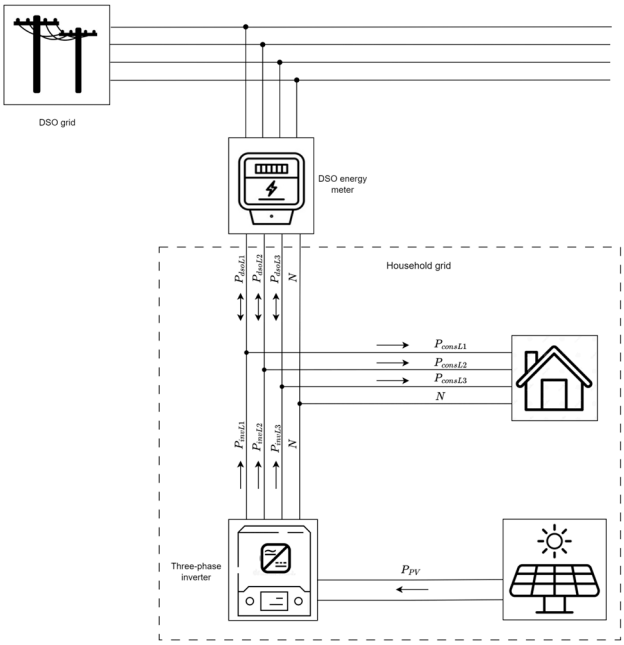


**Figure 1.** Structure of the household grid.

Analysis of data from household grid smart meters reveals anomalies: even when a local photovoltaic system generates sufficient power to meet a household's electricity demand, power may still be imported from the DSO grid. This occurs when phase lines in the household grid become highly asymmetrically loaded. In such cases, one heavily loaded phase line may import power while another phase line exports excess power [31].

One of our previous case studies of these simultaneous active power import and export flows [33] revealed quite significant numbers. It showed that in different households, the annual overlap of imported and exported energy ranges from roughly 6% to 18%, with certain days showing overlap of 60% or more. Moreover, the highest overlaps were observed in households with the smallest installed capacities, and this overlap decreased as installed capacity increased.

Standard DSO smart meters only provide records of cumulative data at hourly intervals, which limits the ability to precisely analyze imported and exported power flows on a short-term basis. In our previous work [32], power flow overlap was examined using smart meters with one-second time resolution. These high-resolution data revealed that roughly half of bidirectional energy flows are caused by asymmetric, time-varying phase loads in the three-phase household grid. The other half emerges from changes in solar irradiation or the activation of high-power single-phase loads within an hour. The study further demonstrated that the operating modes of household three-phase grids can change rapidly over time. As grid loads fluctuate, the ratio of imported to exported power in the three-phase lines can change multiple times per minute. Consequently, one-hour resolution measurements fail to capture these dynamics accurately. By using one-second resolution data, the influence of slow-changing factors—like solar intensity shifts and load switching—can be filtered out, revealing that asymmetric phase loading remains the primary cause of simultaneous bidirectional power flows.

One earlier study [31] proposed a concept of an asymmetrical inverter to deal with the issues caused by load unbalance within phase lines. Standard solar string inverters, widely used in small prosumer households due to their low cost and easy installation, typically operate in symmetric mode. They distribute generated power evenly across all three-phase lines in the household grid, regardless of individual line loads [34–36]. The energy flows and resulting anomalies associated with solar string inverters have been examined in detail by the authors in a previous study [32]. Later advancements in inverter technology have led to the emergence of hybrid solar inverters equipped with smart meters [37–39]. These inverters can operate in asymmetric mode without neutral wire, distributing power unevenly across the three-phase household grid lines, thereby improving the utilization of locally generated photovoltaic energy. However, hybrid solar inverter solutions offered by manufacturers only partially enhance the efficiency of local photovoltaic energy utilization. This partial efficiency gain occurs only when the generated photovoltaic energy is sufficient to meet the household's entire demand at that moment. If the generated energy falls short, and one phase line's load exceeds the combined load of the other two, the hybrid inverter cannot completely eliminate simultaneous active power import and export flows. This imbalance, where one phase line's load surpasses the combined loads of the other two, is common in small prosumer grids, which typically feature only single-phase household appliances. Due to technical constraints, a standard three-phase hybrid solar inverter with a smart meter cannot channel all its output energy into a single phase. Thus, even when photovoltaic generation is adequate to cover the household's energy demand, some imbalance in phase line import and export flows will persist.

This paper further investigates the unique challenges faced by individual prosumers and explores a potential solar inverter control algorithm. The proposed approach aims to fully address simultaneous bidirectional power flows caused by load imbalances across phase lines in the prosumer's household grid.

## 3. Inverter Control Algorithm

As was mentioned above, a typical structure of a three-phase household grid is shown in Figure 1. It comprises a solar power plant, a three-phase inverter, and household loads.

The household grid connects to the DSO grid through a standard DSO energy meter. The figure shows the power flows occurring during the operation.

In each instance, the total power generated by the solar power plant at the inverter's output, excluding the small power consumed by the inverter itself, is as follows:

$$P_{inv} = P_{invL1} + P_{invL2} + P_{invL3} = \sum_{i=1}^{3} P_{invLi}, \quad (1)$$

where $P_{invL1}$, $P_{invL2}$, and $P_{invL3}$ are the power in the corresponding three-phase output lines $L1$, $L2$, and $L3$ of the inverter. Similarly, in each instance, the total power consumed in the household $P_{cons}$ is the sum of the load powers in the three-phase lines $L1$, $L2$, and $L3$.

$$P_{cons} = \sum_{i=1}^{3} P_{consLi}, \quad (2)$$

and the sum of the powers in the lines connected to the DSO grid constitutes the total power $P_{dso}$:

$$P_{dso} = \sum_{i=1}^{3} P_{dsoLi}. \quad (3)$$

Depending on the situation, the power in each three-phase line connected to the DSO grid—$P_{dsoL1}$, $P_{dsoL2}$, and $P_{dsoL3}$—can either be supplied to the household grid (imported) or exported to the DSO grid in case the solar power plant generates excess power. If $P_{dsoLi} > P_{invLi}$, energy is imported on the $i$-th line $Li$ ($i = 1, 2, 3$), and if $P_{dsoLi} < P_{invLi}$, energy is exported. Consequently, a standard symmetric mode inverter can lead to situations where some phase lines import energy while others export it. To prevent this, the three-phase inverter should adaptively assess load changes on each household phase line over time and adjust power management for each inverter output phase line accordingly.

The adaptive power flow management (APFM) algorithm for solar inverters, developed by the authors, is illustrated in Figure 2. At each time reference period $\Delta t$, the algorithm takes as input the power values for all three-phase line loads—$P_{consL1}$, $P_{consL2}$, and $P_{consL3}$—and the total inverter output power $P_{inv}$.

First, the power values of all three loads are sorted in ascending order:

$$P_{Lmax} = max(P_{consL1}, P_{consL2}, P_{consL3}), \quad (4)$$

$$P_{Lmed} = med(P_{consL1}, P_{consL2}, P_{consL3}), \quad (5)$$

$$P_{Lmin} = min(P_{consL1}, P_{consL2}, P_{consL3}). \quad (6)$$

The phase line indices, indicating which phase line each of the sorted power values belongs to, are then recorded:

$$imax = \arg P_{Lmax}, \quad (7)$$

$$imed = \arg P_{Lmed}, \quad (8)$$

$$imin = \arg P_{Lmin}. \quad (9)$$

The imbalance of phase line loads is evaluated by the differences between the power values of the phase line loads:

$$dif1 = P_{max} - P_{med}, \quad (10)$$

$$dif2 = P_{med} - P_{min}. \quad (11)$$

The algorithm's operation is divided into three cases, depending on the power generated by the solar power plant and the load consumption. In the first case, if $P_{inv} \leq dif1$ (indicating that the solar power plant is generating relatively little power), all generated

power is directed to the most heavily loaded phase line, with no power allocated to the other two lines:

$$P_{Lmax} = P_{inv}, P_{Lmed} = 0, P_{Lmin} = 0. \quad (12)$$

In the second case, if the solar power plant generates more power and satisfies the condition $dif1 < P_{inv} \leq dif1 + 2dif2$, the generated power is distributed between the two most heavily loaded phase lines, while the least loaded phase line receives no power:

$$P_{Lmax} = dif1 + (P_{inv} - dif1)/2, P_{Lmed} = (P_{inv} - dif1)/2, P_{Lmin} = 0. \quad (13)$$

In the third case, when the power generated by the solar power plant is high, i.e., when $P_{inv} > dif1 + 2dif2$, this power is distributed between all three-phase lines according to the following rules:

$$P_{Lmax} = dif1 + dif2 + (P_{inv} - dif1 - 2dif2)/3, P_{Lmed} = dif2 + (P_{inv} - dif1 - 2dif2)/3, P_{Lmin} = (P_{inv} - dif1 - 2dif2)/3. \quad (14)$$

By redistributing the powers in this way and restoring the three-phase line indices {*imax*, *imed*, *imin*} => {1, 2, 3} according to Formulas (7)–(9), new inverter output power values $P\prime_{invL1}$, $P\prime_{invL2}$, and $P\prime_{invL3}$ are obtained (here and below, power values after redistribution are marked with an apostrophe).

The pseudocode of the proposed APFM algorithm is given below.

Step 1. Read the household load power data of each phase line $P_{consL1}$, $P_{consL2}$, $P_{consL3}$, as well as the total inverter output power $P_{inv}$.

Step 2. Sort the phase load powers $P_{consLi}$ ($i$ = 1, 2, 3) in descending order to determine the values of $P_{Lmax}$, $P_{Lmed}$, $P_{Lmin}$ for each phase line using Formulas (4)–(6).

Step 3. Define indexes *imin*, *imed*, and *imax* of the phase lines corresponding to $P_{Lmax}$, $P_{Lmed}$, $P_{Lmin}$, according to Formulas (7), (8), and (9).

Step 4. Calculate the differences between the power values of the phase line loads $dif1$, $dif2$ using Formulas (10) and (11).

Step 5. If $P_{inv} \leq dif1$, apply Formula (12) to calculate the new values of $P_{Lmin}$, $P_{Lmed}$, $P_{Lmax}$, and go to Step 8, otherwise go to the next step.

Step 6. If $dif1 < P_{inv} \leq dif1 + 2 \times dif2$, apply Formula (13) to calculate the new values of $P_{Lmin}$, $P_{Lmed}$, $P_{Lmax}$, and go to Step 8, otherwise go to the next step.

Step 7. Apply Formula (14) to calculate new values of $P_{Lmin}$, $P_{Lmed}$, $P_{Lmax}$.

Step 8. Assign power $P'_{invLimax}$ to $P_{Lmax}$, power $P'_{invLimed}$ to $P_{Lmed}$, power $P'_{invLimin}$ to $P_{Lmin}$.

Step 9. Assign power values $P'_{invLimax}$, $P'_{invLimed}$, and $P'_{invLimin}$ to the PV inverter outputs of each phase line $P'_{invL1}$, $P'_{invL2}$, and $P'_{invL3}$ according to index relations defined in Step 3.

This algorithm ensures that all the energy provided by the inverter is primarily used for load balancing within the phase lines. Figure 3 shows possible cases of power redistribution in household three-phase lines when the algorithm is running: power in load lines, when the solar power plant is not generating (a), power in the output lines of a three-phase inverter and household load lines, when solar power is low compared to the load power (b), when solar power is average compared to the load power (c), and when solar power is high compared to the load power, but still below the total load power (d). The orange color represents the total power generated by the solar power plant, the red, green, and blue colors represent the portions of the solar power redistributed by the inverter, and the black represents the power imported by the household from the DSO grid.

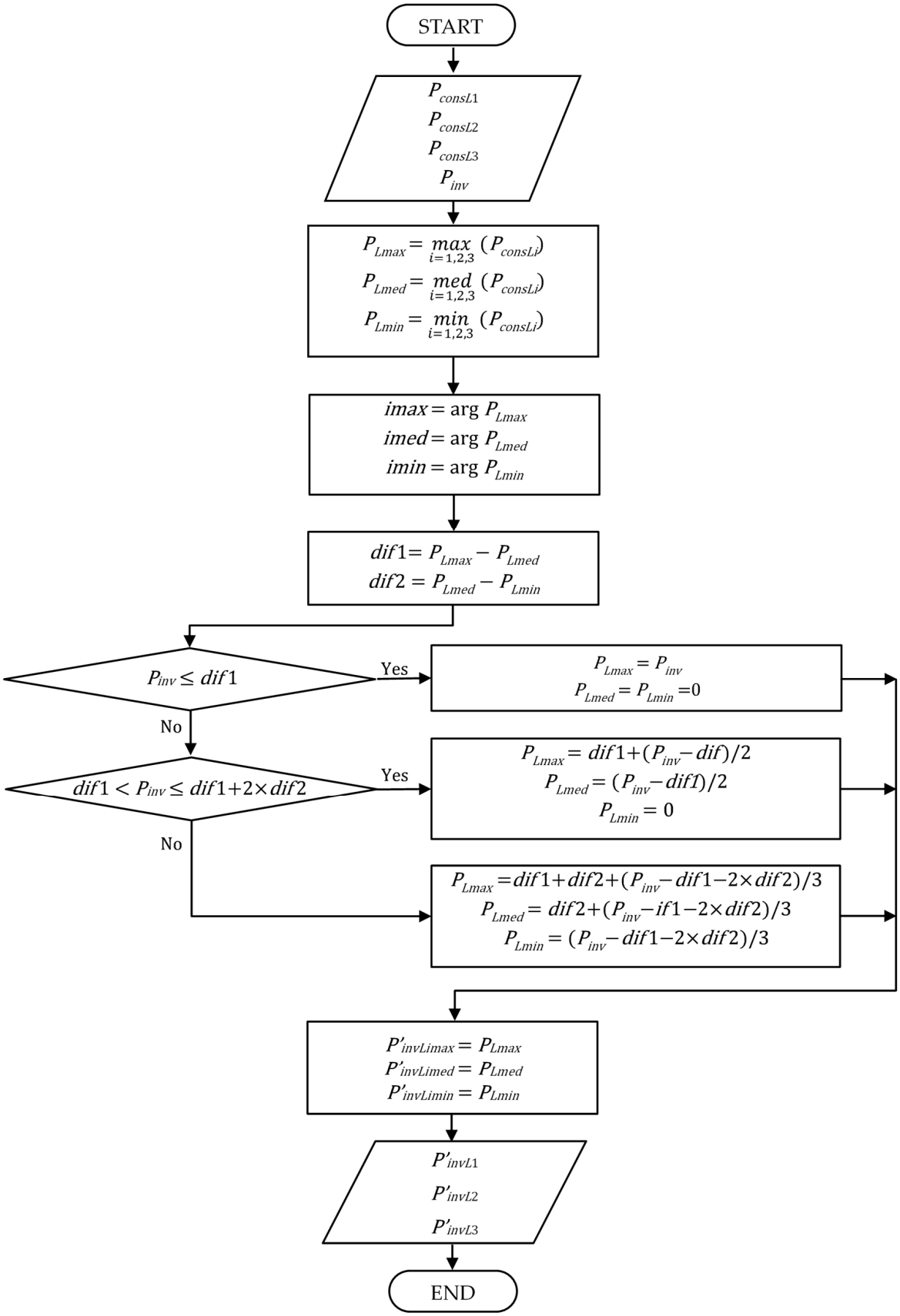


**Figure 2.** APFM algorithm.

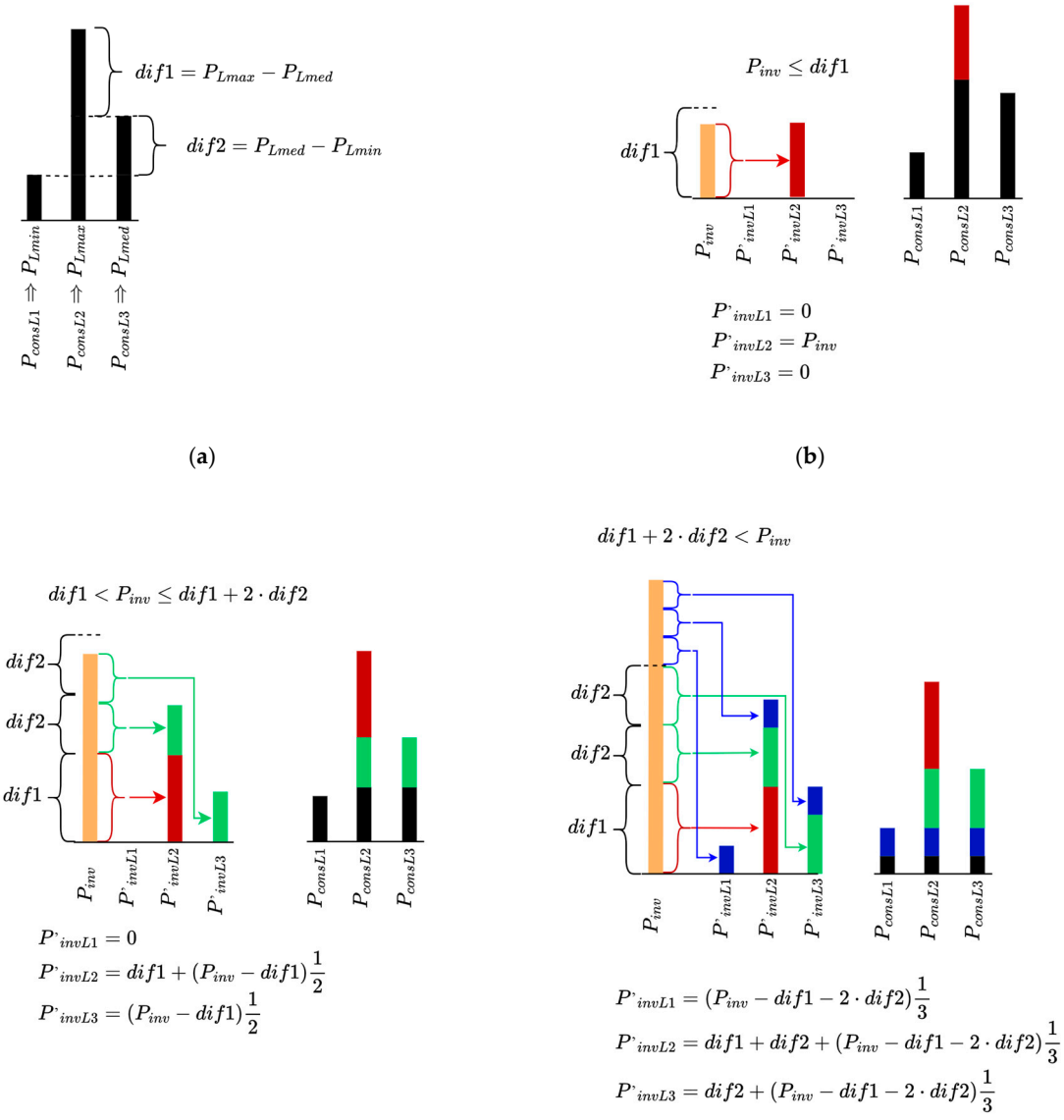


**Figure 3.** Inverter and load power distribution diagrams for various PV generation cases when: the solar power plant is not generating (**a**), solar inverter output power is low (**b**), moderate (**c**) and high (**d**) compared to the load power.

## 4. Simulation Results

The proposed algorithm was tested using real household data. A measurement system with two additional smart three-phase electricity meters was installed in a 20 kWp household grid powered by a 10 kWp solar power plant [32]. These two meters recorded the average active power flows at one-second intervals ($\Delta t$ = 1 s). One of those meters measured bidirectional—imported and exported—power on the edge of the DSO grid in three-phase lines—$P_{dsoL1}$, $P_{dsoL2}$, and $P_{dsoL3}$,—while another meter tracked power flows from the solar plant's three-phase symmetric mode inverter outputs—$P_{invL1}$, $P_{invL2}$, and $P_{invL3}$. Each sample of measured data from the meters was transmitted to an SQL server in real time and stored for later analysis. The data collection took place from April to October 2023. The load power flow (consumption) in each phase line $P_{consLi}$ was derived from the measured data:

$$P_{consLi} = P_{invLi} - P_{dsoLi}, \quad (15)$$

where $i$ = 1, 2, 3. Besides, $P_{dsoLi}$ is positive when power is exported in the $i$-th phase line, and negative when power is imported.

The operation of the household grid was simulated, analyzed, and visualized using MATLAB/Simulink R2023a, both with and without the proposed APFM algorithm. During the simulation of the APFM algorithm, real three-phase output data from the symmetrical household inverter $P_{invLi}$ and data from the lines connected to the DSO grid $P_{dsoLi}$ were used for each one-second time interval. Using these real data, the total power generated by the solar power plant $P_{inv}$ (1) and the consumption power in each phase line $P_{consLi}$ (15) were calculated and used as input for the APFM algorithm. The input data were then processed into output data by the APFM algorithm using a MATLAB/Simulink model.

To evaluate the effectiveness of the APFM algorithm, simulated output data of the three-phase asymmetric mode inverter with neutral wire aided by the proposed algorithm were compared with the measured symmetric mode inverter output data over the course of each day, using the same measured real household data. The full analysis focused on typical situations over the selected eleven days.

For visualization of the simulation results, the two most extreme cases (6 June and 15 April) were selected. The power flow profiles for these days are displayed in Figures 4–6. Active power is measured in watts, and time is shown in seconds, starting from midnight (00:00). Figure 4 presents the household load (consumption) power flows, calculated as per (15), for the three-phase lines: $P_{consL1}$ (blue), $P_{consL2}$ (red), and $P_{consL3}$ (yellow).

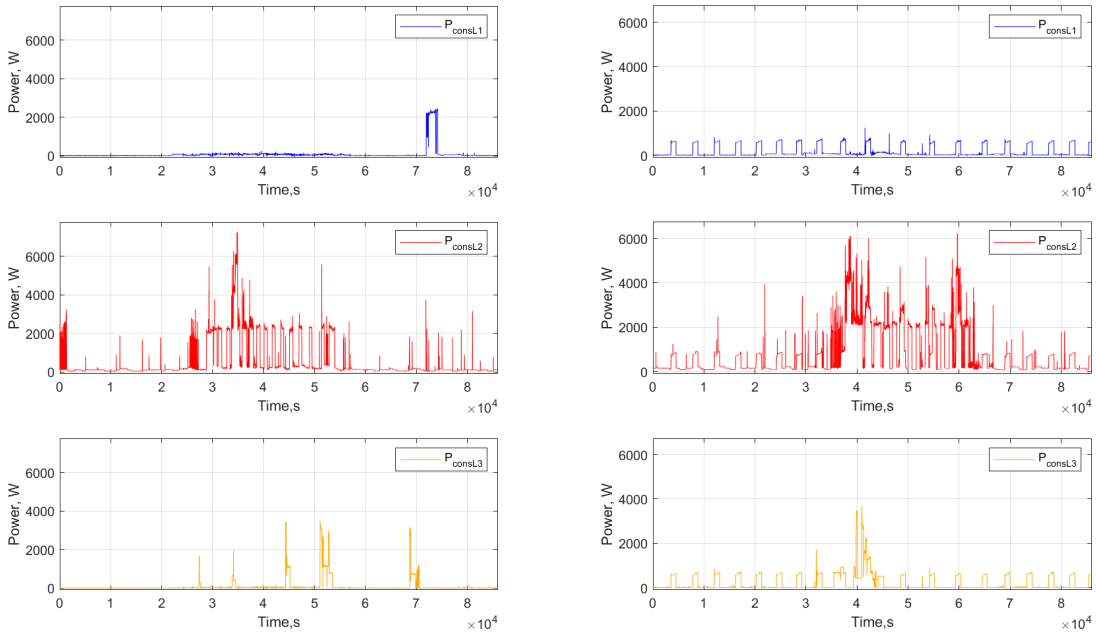


**Figure 4.** Household load power flows in phase lines $P_{consL1}$, $P_{consL2}$, and $P_{consL3}$ for 6 June (**a**) and 15 April (**b**).

In both cases the household grid's three-phase lines are unevenly loaded. On 6 June (Figure 4a), line $L2$ carries the heaviest load, particularly during the day, while line $L3$ handles short-term loads mainly in daylight hours, and line $L1$ has a steady load of about 2 kW in the evening. On 15 April (Figure 4b), line $L2$ remains the most heavily loaded line, but the additional three-phase load is periodically drawing power from all three lines throughout the day.

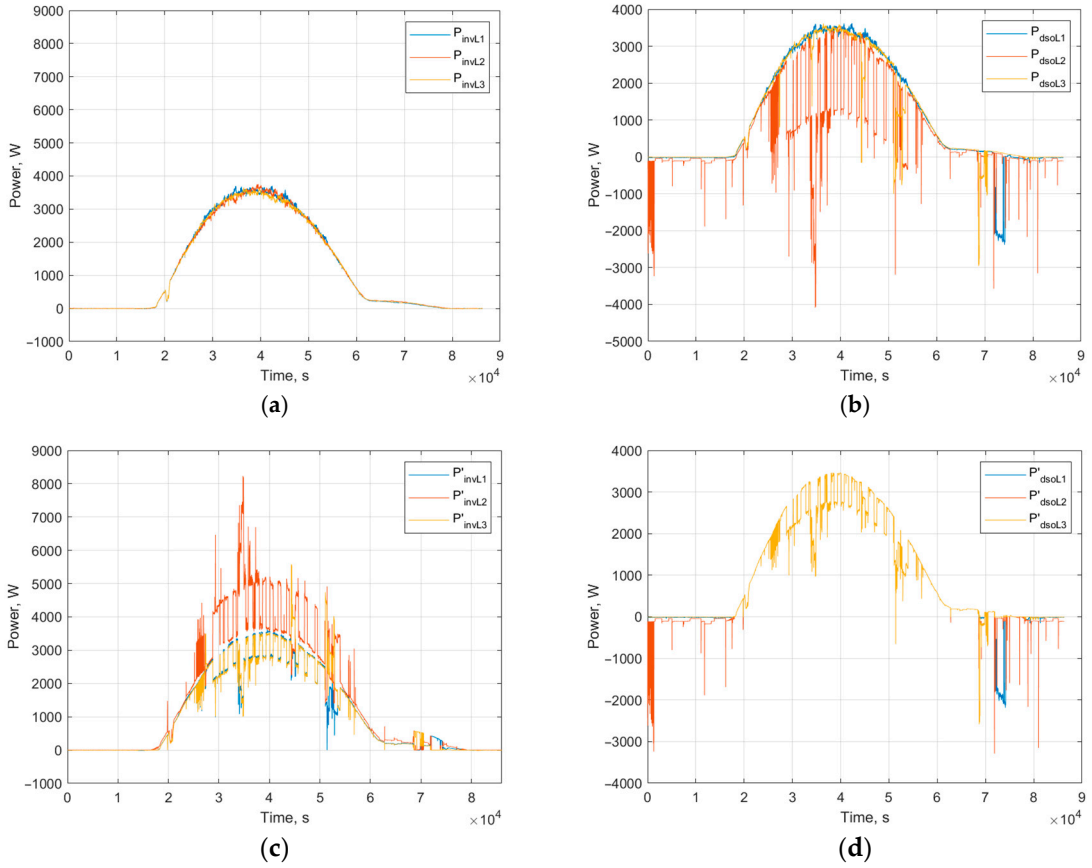


**Figure 5.** Power flow profiles in the household grid throughout the day on 6 June: inverter output power flows for symmetric (**a**) and simulated asymmetric (**c**) modes, and imported—exported power flows for symmetric (**b**) and simulated asymmetric (**d**) modes.

Figure 5 shows examples of the household grid's power flow profiles on 6 June: with the inverter operating symmetrically (Figure 5a,b) and with the simulated adaptive asymmetric mode inverter in use (Figure 5c,d). Figure 5a displays the solar power plant's generation profiles throughout the day. These profiles are consistent, indicating sunny, cloudless conditions. With the inverter in symmetric mode, the power profiles for the three-phase outputs—$P_{invL1}$ (blue), $P_{invL2}$ (red), and $P_{invL3}$ (yellow)—are virtually identical. (In this and the next figures, when all three-phase line profiles fully overlap, red may cover blue, and yellow may cover both red and blue.)

Figure 5b shows the imported and exported power flows in each phase line on 6 June, using the same color coding: $P_{dsoL1}$ (blue), $P_{dsoL2}$ (red), $P_{dsoL3}$ (yellow). Exported power is shown as positive values, while imported power is shown as negative values. This figure illustrates the impact of solar generation and household load on the three-phase household grid lines.

Comparing Figure 5a,b, it becomes clear that when solar generation is absent, all the energy consumed by the household is imported. On the heavily loaded line $L2$ (red), even when the solar power plant generates more than 3 kW in each phase line, significant power imports still occur at certain times. In contrast, such instances are rare on line $L3$ (yellow) and completely absent on line $L1$ (blue).

Figure 5c shows the simulated power flows for the three-phase lines $P'_{invL1}$, $P'_{invL2}$, and $P'_{invL3}$ with the APFM algorithm in use. A comparison with the load profiles in Figure 4a clearly demonstrates how the inverter adjusts to the changing loads in the grid. Consequently, when the solar power plant generation is relatively high, imported power flows are nearly eliminated (Figure 6d).

Figure 6, similar to Figure 5, presents the household grid power flows for 15 April. The picture shows the inverter output power flows $P_{invL1}$, $P_{invL2}$, and $P_{invL3}$ (a) and imported and exported power flows $P_{dsoL1}$, $P_{dsoL2}$, and $P_{dsoL3}$ (b), when the three-phase inverter operates in the symmetric mode, and the simulated inverter output power flows $P'_{invL1}$, $P'_{invL2}$, and $P_{invL3}$ (c) and imported and exported power flows $P'_{dsoL1}$, $P'_{dsoL2}$, and $P'_{dsoL3}$ (d), when the three-phase inverter operates in the adaptive asymmetric mode. In this case, solar generation is limited, and the symmetric mode inverter generates significantly less power per phase line throughout the day (Figure 6a) compared to 6 June (Figure 5a). At the same time, the phase lines are more heavily loaded than in the previously analyzed example (see Figure 4). Consequently, with the symmetric mode inverter, a notable portion of power—especially on the lines *L*2 and *L*3—is imported even when solar power is being generated (Figure 6b). However, in the simulated adaptive asymmetric inverter mode (Figure 6d), such occurrences are significantly reduced.

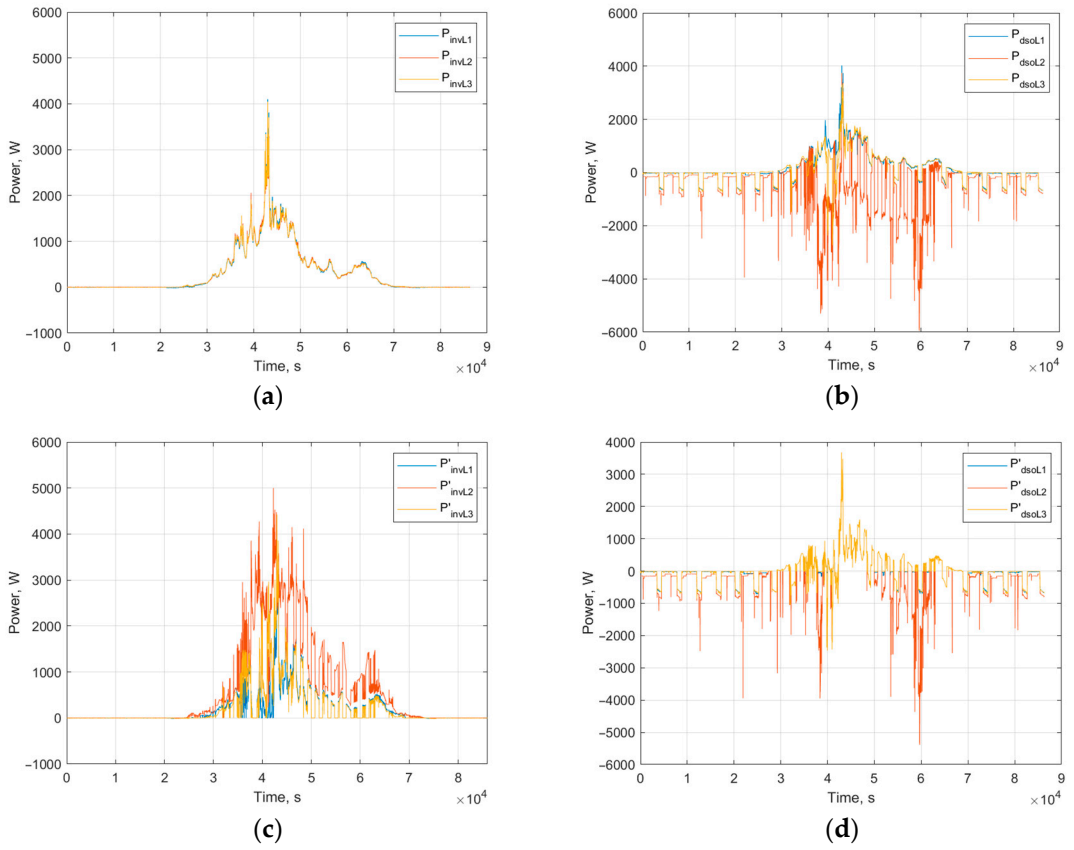


**Figure 6.** Power flow profiles in the household grid throughout the day on 15 April: inverter output power flows for symmetric (**a**) and simulated asymmetric (**c**) modes, and imported—exported power flows for symmetric (**b**) and simulated asymmetric (**d**) modes.

In the symmetric inverter operating mode, the power imported from the DSO grid in the *i*-th phase line during each *j*-th second is obtained as follows:

$$P_{impLi} = \begin{cases} |P_{dsoLi}|, & if \;\; P_{dsoLi} < 0, \\ 0, & otherwise, \end{cases} \tag{16}$$

where $i = 1,\ 2,\ 3$.

Similarly, in the adaptive asymmetric mode, it is obtained as follows:

$$P'_{impLi} = \begin{cases} |P'_{dsoLi}|, & if \;\; P'_{dsoLi} \leq 0, \\ 0, & otherwise. \end{cases} \tag{17}$$

The total imported power in all three-phase lines for both symmetric and asymmetric modes is obtained as follows:

$$P_{imp} = P_{impL1} + P_{impL2} + P_{impL3}, \tag{18}$$

$$P'_{imp} = P'_{impL1} + P'_{impL2} + P'_{impL3}. \tag{19}$$

It is obvious, from the previous examples, that applying the proposed algorithm allows more efficient use of solar power in the household, meaning less energy is imported and imported. The reduction in export can be quantified by the parameter $\Delta P_{imp}$:

$$\Delta P_{imp} = P_{imp} - P'_{imp}. \tag{20}$$

The distribution of this parameter throughout the day on the selected days of 15 April and 6 June is shown in Figure 7.

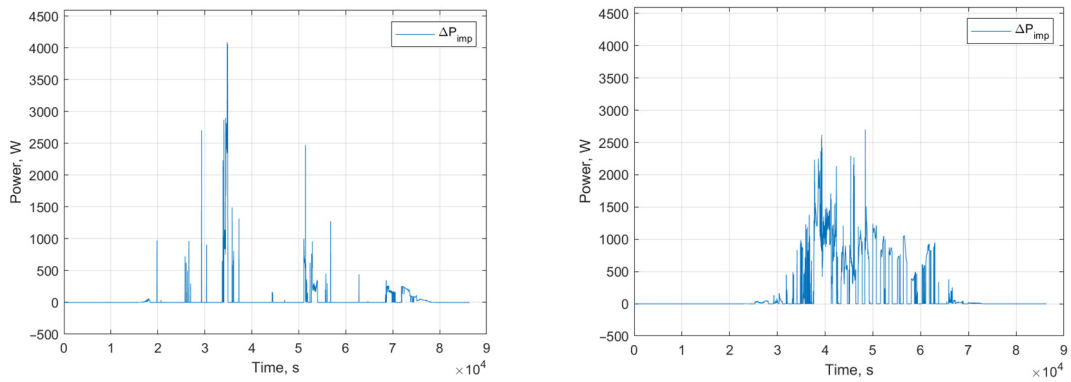


**Figure 7.** The reduction in imported power $\Delta P_{imp}$ throughout the day when applying the asymmetric mode inverter with the APFM algorithm instead of the symmetric inverter on 6 June (**a**) and 15 April (**b**).

It should be noted that the reduction in imported power is exactly matched by a reduction in exported power to the DSO grid, meaning $\Delta P_{exp} = \Delta P_{imp}$. This is because the power is consumed locally, rather than sent to or drawn from the DSO grid. Consequently, simultaneous bidirectional power flows between the DSO and the household grid are reduced. In scenarios with abundant solar energy and relatively low loads (6 June), the adaptive asymmetric inverter mode is less efficient (Figure 7a) compared to days with lower solar generation and higher loads (15 April, Figure 7b).

To determine the total daily reduction in power flows, all $\Delta P_{imp}$ values for each second of the day are summed. This total represents the energy saved during the day, expressed in watt-seconds (Ws), which can then be converted into more familiar form—kilowatt-hours (kWh):

$$\Delta E_{IMP} = \frac{\sum_{j=1}^{N} \Delta P_{impj}}{H \cdot 10^3}, \tag{21}$$

where $N$ is the number of seconds in a day ($N$ = 86,400), and $H$ is the number of seconds in an hour ($H$ = 3600). The decrease in exported energy is calculated in a similar way:

$$\Delta E_{EXP} = \frac{\sum_{j=1}^{N} \Delta P_{expj}}{H \cdot 10^3}. \quad (22)$$

As previously noted, the reductions in both exported and imported power are equal, so the reductions in imported and exported energy are also equal: $\Delta E_{EXP} = \Delta E_{IMP}$.

Table 1 shows the calculated reductions in imported ($\Delta E_{IMP}$) and exported ($\Delta E_{EXP}$) energy for the household across 11 selected days. It also includes the total daily imported flows when the inverter is operating in symmetric mode:

$$E_{IMP} = \frac{\sum_{j=1}^{N} P_{impj}}{H \cdot 10^3}, \quad (23)$$

and when the inverter operates in adaptive asymmetric mode, the calculation is as follows:

$$E'_{IMP} = \frac{\sum_{j=1}^{N} P'_{impj}}{H \cdot 10^3}. \quad (24)$$

Additionally, the table provides the daily energy consumed by the household and generated by the solar power plant, calculated by summing the consumption ($P_{cons}$) and generation ($P_{inv}$) for each $j$-th second across all three-phase lines throughout the day:

$$E_{CONS} = \frac{\sum_{j=1}^{N} P_{consj}}{H \cdot 10^3}, \quad (25)$$

$$E_{INV} = \frac{\sum_{j=1}^{N} P_{invj}}{H \cdot 10^3}. \quad (26)$$

**Table 1.** Comparison of household grid energy flows simulated for both symmetric and adaptive asymmetric inverter modes throughout the preselected days.

| Day | Consumed Energy $E_{CONS}$, kWh | Generated Energy $E_{INV}$, kWh | Symmetric Mode Imported Energy $E_{IMP}$, kWh | Asymmetric Mode Imported Energy $E'_{IMP}$, kWh | Symmetric Mode Exported Energy $E_{EXP}$, kWh | Asymmetric Mode Exported Energy $E'_{EXP}$, kWh | Change in Energy Flows $\Delta E_{IMP}$, $\Delta E_{EXP}$, kWh |
|---|---|---|---|---|---|---|---|
| 9 April 2023 | 25.3196 | 43.8237 | 14.1781 | 10.9305 | 32.6823 | 29.4347 | 3.2476 |
| 15 April 2023 | 26.4319 | 23.1373 | 17.1283 | 13.2877 | 13.8336 | 9.9931 | 3.8405 |
| 20 April 2023 | 26.3170 | 69.1036 | 9.9760 | 7.8981 | 52.7626 | 50.6847 | 2.0779 |
| 5 May 2023 | 23.4818 | 80.4442 | 10.7783 | 10.2962 | 67.7407 | 67.2586 | 0.4821 |
| 12 May 2023 | 18.4194 | 81.0061 | 8.6393 | 7.7396 | 71.2260 | 70.3264 | 0.8996 |
| 27 May 2023 | 13.6880 | 83.2921 | 5.2018 | 4.3365 | 74.8059 | 73.9406 | 0.8653 |
| 6 June 2023 | 16.4728 | 87.2927 | 3.4029 | 2.4247 | 74.2228 | 73.2446 | 0.9782 |
| 18 June 2023 | 16.3668 | 30.4403 | 9.4676 | 4.7885 | 23.5412 | 18.8620 | 4.6792 |
| 24 June 2023 | 6.5271 | 63.1811 | 1.3270 | 0.8212 | 57.9810 | 57.4752 | 0.5058 |
| 1 July 2023 | 13.2809 | 60.1049 | 3.9824 | 1.7570 | 50.8065 | 48.5810 | 2.2255 |
| 23 September 2023 | 14.6520 | 40.9598 | 5.4307 | 3.6268 | 31.7385 | 29.9346 | 1.8039 |

From the data in the table, it is evident that the asymmetric inverter mode, using the authors' proposed algorithm, reduces both imported energy ($E'_{IMP}$) and exported energy ($E'_{EXP}$) compared to the conventional symmetric inverter mode. The efficiency of this operating mode, measured by the parameters $\Delta E_{IMP}$ and $\Delta E_{EXP}$, depends on the solar-generated power and the total household grid load. For this particular household grid,

analyzed over the spring, summer, and autumn periods, the load remained relatively stable. As a result, it can be concluded that the asymmetric inverter mode control algorithm is more efficient during lower solar generation levels than higher ones: the higher $\Delta E_{IMP}$ and $\Delta E_{EXP}$ values correspond to lower $E_{INV}$ values. This efficiency is especially apparent in the 15 April example, where household consumption exceeded generation (about 23.14 kWh and 26.43 kWh, respectively), leading to a reduction of 3.84 kWh in both imported and exported energy. In contrast, during periods of higher solar generation or lower consumption (such as on 24 June), these energy flow reductions were limited to under 1 kWh.

An asymmetric three-phase load degrades the DSO grid's performance. Households often load such a grid unevenly, causing significant differences in power flows across the phase lines. This grid imbalance is measured using the relative power imbalance parameter ($RP_{imb}$), which represents the maximum power difference between grid lines relative to the household's contracted power. In the case of a symmetric mode inverter, for each $j$-th second the relative power imbalance parameter is as follows:

$$RP_{imb} = \frac{\max\limits_{i=1,2,3} P_{dsoLi} - \min\limits_{i=1,2,3} P_{dsoLi}}{P_{inst}} \cdot 100\%, \tag{27}$$

where $P_{inst}$ is the household's contracted power. In the case of the adaptive asymmetric inverter mode, it is as follows:

$$RP'_{imb} = \frac{\max\limits_{i=1,2,3} P'_{dsoLi} - \min\limits_{i=1,2,3} P'_{dsoLi}}{P_{inst}} \cdot 100\%. \tag{28}$$

The variations in these parameters over 6 June and 15 April are shown in Figure 8. As shown, the symmetric mode inverter significantly unbalances the grid during solar generation (Figure 8, top), as it does not adapt to load variations across the phase lines. In contrast, the adaptive asymmetric mode inverter (Figure 8, middle) mostly avoids such imbalances, with imbalance only occurring when solar generation is insufficient.

The difference between $RP_{imb}$ and $RP'_{imb}$, denoted as $\Delta RP_{imb} = RP_{imb} - RP'_{imb}$, quantifies how much the proposed adaptive inverter reduces phase line power imbalance compared to a conventional symmetric inverter. Figure 8 provides an example from 15 April, a day with lower solar generation and higher loads. In this case, the adaptive asymmetric inverter (Figure 8, middle) fully balances the grid, but solar generation is only sufficient for a short period around midday. Despite solar generation being limited, the overall grid imbalance improves, as reflected in the $\Delta RP_{imb}$ parameter (Figure 8, bottom).

The total daily imbalance for both symmetric and asymmetric mode inverters was evaluated by averaging the individual imbalances throughout the day:

$$RP_{IMB} = \frac{\sum_{j=1}^{N} RP_{imbj}}{N}, \tag{29}$$

$$RP'_{IMB} = \frac{\sum_{j=1}^{N} RP'_{imbj}}{N}. \tag{30}$$

The values of these parameters, derived from analyzing data from 11 preselected days, are shown in Table 2. The table also includes the percentage reduction in overall daily imbalance ($\Delta RP_{IMB} = RP_{IMB} - RP'_{IMB}$) and the reduction factor ($RPT_{IMB} = RP_{IMB}/RP'_{IMB}$), comparing the adaptive asymmetric mode inverter's operation to that of the symmetric mode inverter. As indicated by the research results, the daily average imbalance never exceeded 1% when the adaptive asymmetric mode inverter was in use.

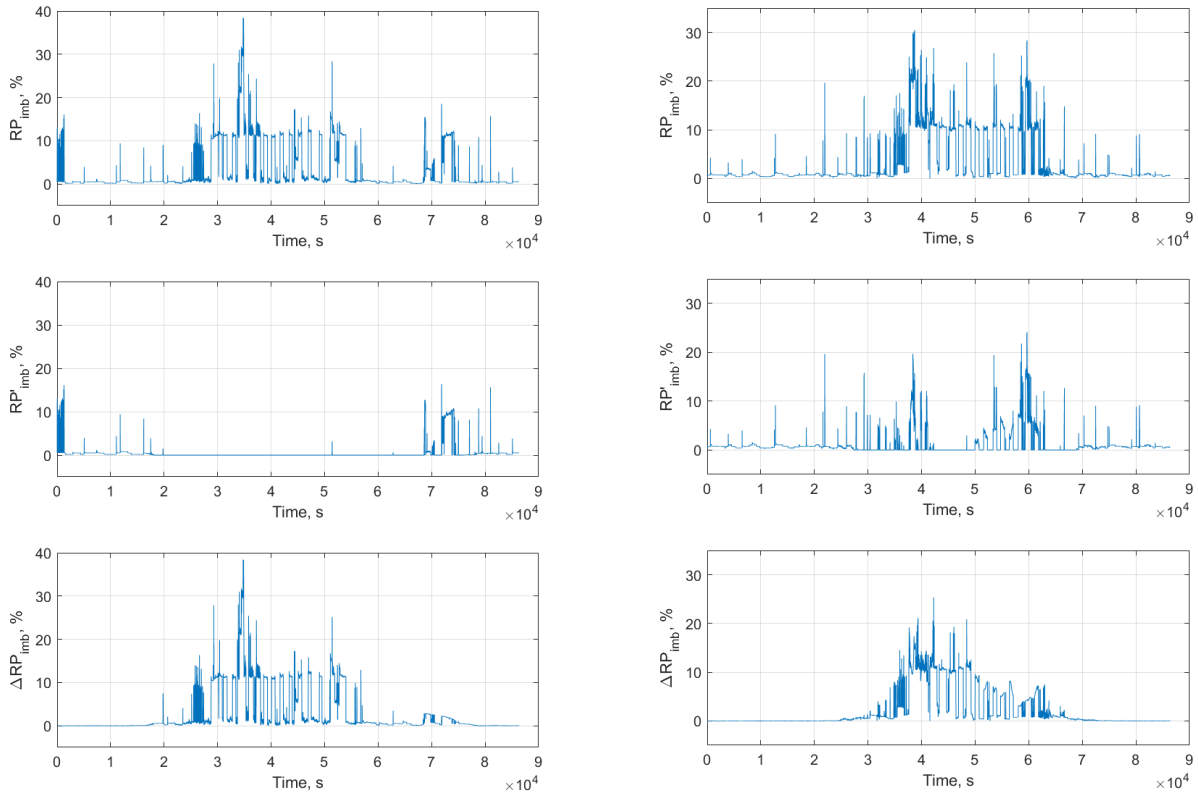


**Figure 8.** The change in relative power imbalances $RP_{imb}$ (**top**) and $RP'_{imb}$ (**middle**) and their difference $\Delta RP_{imb}$ (**bottom**) throughout the day on 6 June (**a**) and 15 April (**b**).

**Table 2.** The daily averages of household three-phase line imbalances and their comparison in the case of symmetric and asymmetric inverters.

| Day | Average Daily Imbalance | | Decreases in Imbalance | |
|---|---|---|---|---|
| | Symmetric Mode $RP_{IMB}$, % | Asymmetric Mode $RP'_{IMB}$, % | $\Delta RP_{IMB}$, % | $RPT_{IMB}$ |
| 9 April 2023 | 3.18 | 0.81 | 2.37 | 3.92 |
| 15 April 2023 | 2.95 | 0.91 | 2.04 | 3.23 |
| 20 April 2023 | 3.55 | 0.49 | 3.06 | 7.25 |
| 5 May 2023 | 1.99 | 0.34 | 1.65 | 5.84 |
| 12 May 2023 | 2.78 | 0.74 | 2.04 | 3.78 |
| 27 May 2023 | 2.51 | 0.80 | 1.71 | 3.14 |
| 6 June 2023 | 2.99 | 0.42 | 2.57 | 7.09 |
| 18 June 2023 | 3.05 | 0.73 | 2.32 | 4.16 |
| 24 June 2023 | 1.19 | 0.13 | 1.06 | 9.27 |
| 1 July 2023 | 2.39 | 0.22 | 2.17 | 11.02 |
| 23 September 2023 | 2.42 | 0.45 | 1.97 | 5.34 |

In contrast, for the symmetric mode inverter, it was between 3.14 and 11.02 (on average 5.8) times higher, exceeding 3% in some cases (3.05% on 18 June, 3.18% on 9 April, and 3.55% on 20 April).

In the literature, the efficiency of systems with local energy generation sources is often evaluated using the self-sufficiency rate (*SSR*) and the self-consumption rate (*SCR*) [22,25,32,40,41]. The first indicator, *SSR*, measures the percentage of energy consumed from local generation sources relative to the total system consumption, calculated

over a given period (e.g., a day). The second indicator, *SCR*, measures the percentage of locally generated and consumed energy relative to the total locally generated energy, also measured over a specific period.

For the analyzed 11-day cases, *SSR* and *SCR* were calculated for scenarios where the inverter operates in the symmetric and adaptive asymmetric modes. In the symmetric mode, *SSR* was determined using the following formula:

$$SSR = \frac{E_{CONS} - E_{IMP}}{E_{CONS}} \cdot 100\%, \tag{31}$$

and the *SCR* was calculated using the following formula:

$$SCR = \frac{E_{INV} - E_{EXP}}{E_{INV}} \cdot 100\%. \tag{32}$$

Similarly, these indicators were calculated for the case where the inverter operates in the adaptive asymmetric mode, using the following formulas:

$$SSR' = \frac{E_{CONS} - E'_{IMP}}{E_{CONS}} \cdot 100\%, \tag{33}$$

$$SCR' = \frac{E_{INV} - E'_{EXP}}{E_{INV}} \cdot 100\%. \tag{34}$$

When comparing the indicators for both modes on the same day, the same consumed energy ($E_{CONS}$) and solar-generated energy ($E_{INV}$) are used. Therefore, difference in values of those indicators might appear only because of variation in imported or exported electricity, e.g., reducing of imported/exported electricity results in increase of those indicators, meaning the more efficient utilization of the solar-generated energy.

Table 3 lists the calculated self-sufficiency rate (*SSR*) and self-consumption rate (*SCR*) indicators for both the symmetric and adaptive asymmetric inverter modes during the analyzed 11-day cases. The table also includes the percentage improvement in these indicators under the adaptive asymmetric mode, calculated as follows:

$$\Delta SCR = SCR - SCR', \tag{35}$$

$$\Delta SSR = SSR - SSR'. \tag{36}$$

The *SCR* improvement depends not only on the solar plant's energy generation $E_{INV}$ but also on the reduction in exported energy flows $\Delta E_{EXP}$, where $\Delta E_{EXP} = \Delta E_{IMP}$. Similarly, the *SSR* improvement depends on the reduction in imported energy flows $\Delta E_{IMP}$ and the total energy consumed $E_{CONS}$.

Table 3 also includes the reduction in imported energy $\Delta E_{IMP}$, expressed as a percentage of the total daily imported energy amount obtained in the case of the symmetric inverter mode:

$$\Delta E_{IMP\%} = \frac{\Delta E_{IMP}}{E_{IMP}} 100\% \,. \tag{37}$$

As previously mentioned, the improvement in *SCR* and *SSR* values is directly dependent on the reduction in the bidirectional flows $\Delta E_{EXP}$ and $\Delta E_{IMP}$.

When the inverter operated in symmetric mode, the household *SCR* value ranged from 8.23% to 40.21% (on average about 19.2%), while with the asymmetric mode inverter using the proposed algorithm, the *SCR* ranged from 9.03% to 56.81% (on average about 24.2%), representing a 5% improvement. The *SSR* parameter for the symmetric mode ranged from 35.2% to 79.67% (on average about 58.6%), while in the asymmetric mode it ranged from 49.73% to 87.42% (on average about 69.5%), showing an 11% improvement.

The percentage reduction in imported energy ($\Delta E_{IMP\%}$), when the inverter operated in the adaptive asymmetric mode compared to symmetric mode, ranged from 4.5% to 49.4% during the study period, with an average reduction of 27.5% over the entire period.

**Table 3.** Self-consumption rate (*SCR*) and self-sufficiency rate (*SSR*) indicators and their comparison for symmetric and asymmetric inverter operating modes.

| Day | Self-Consumption Rate | | Change in Self-Consumption Rate $\Delta SCR$,% | Self-Sufficiency Rate | | Change in Self-Sufficiency Rate $\Delta SSR$, % | Decrease in Energy Import $\Delta E_{IMP\%}$, % |
|---|---|---|---|---|---|---|---|
| | Symmetric Mode *SCR*, % | Asymmetric Mode $SCR'$, % | | Symmetric Mode *SSR*, % | Asymmetric Mode $SSR'$, % | | |
| 9 April 2023 | 25.42 | 32.83 | 7.41 | 44.00 | 56.83 | 12.83 | 22.9 |
| 15 April 2023 | 40.21 | 56.81 | 16.60 | 35.20 | 49.73 | 14.53 | 22.4 |
| 20 April 2023 | 23.65 | 26.65 | 3.01 | 62.09 | 69.99 | 7.90 | 20.8 |
| 5 May 2023 | 15.79 | 16.39 | 0.60 | 54.10 | 56.15 | 2.05 | 4.5 |
| 12 May 2023 | 12.07 | 13.18 | 1.11 | 53.10 | 57.98 | 4.88 | 10.4 |
| 27 May 2023 | 10.19 | 11.23 | 1.04 | 62.00 | 68.32 | 6.32 | 16.6 |
| 6 June 2023 | 14.97 | 16.09 | 1.12 | 79.34 | 85.28 | 5.94 | 28.7 |
| 18 June 2023 | 22.66 | 38.04 | 15.37 | 42.15 | 70.74 | 28.59 | 49.4 |
| 24 June 2023 | 8.23 | 9.03 | 0.80 | 79.67 | 87.42 | 7.75 | 38.1 |
| 1 July 2023 | 15.47 | 19.17 | 3.70 | 70.01 | 86.77 | 16.76 | 55.9 |
| 23 September 2023 | 22.51 | 26.92 | 4.40 | 62.94 | 75.25 | 12.31 | 33.2 |

The proposed APFM algorithm enables the inverter to distribute solar-generated power unevenly across the household grid three-phase lines every second based on phase loads, which results in more efficient solar energy utilization, reducing both power import and export. Additionally, it makes power export to the DSO grid more symmetrical across all phase lines, improving grid stability and capacity. This active power flow management approach can be implemented in hybrid solar inverters equipped with a neutral wire.

## 5. Discussion

An adaptive asymmetric inverter mode operating under the proposed AFPM algorithm, compared to the conventional symmetric mode, enables more efficient utilization of solar-generated energy within the household. This means more energy would be consumed locally, thereby reducing energy imports. This is achieved due to the adaptability of the AFPM algorithm, which controls the inverter's operation based on load variations in the household grid. It is important to note that in this case, any reduction in imported energy corresponds to an equal reduction in energy exported to the DSO grid, as the energy is consumed locally rather than being sent to or drawn from the DSO grid. This helps minimize simultaneous bidirectional power flows between the DSO and the household grid. An analysis of the same household grid during the spring, summer, and autumn periods showed that the percentage reduction in imported energy, when simulating inverter operation in the adaptive asymmetric mode compared to the symmetric mode, was on average 27.5%. Furthermore, in terms of this reduction parameter, the inverter's asymmetric mode control algorithm was found to be more efficient at lower solar power generation levels than at higher ones.

A symmetric mode inverter, when solar generation is present, also causes an imbalance in the DSO grid, as it does not adapt to the load variations in the household's phase lines. The adaptive asymmetric mode inverter does not introduce such an imbalance, except when solar generation is insufficient. Analyzing this power imbalance revealed that the proposed adaptive inverter mode reduces phase line imbalances compared to the conventional symmetric inverter. In the case of the adaptive asymmetric mode inverter, the daily average imbalance in all investigated cases did not exceed 1%, whereas for the

symmetric mode inverter, it was above 3%. Thus, the inverter operating under the AFPM algorithm ensures that power export to the DSO grid is more symmetrical across all phase lines. This has a highly beneficial effect on the DSO grid infrastructure and minimizes energy transmission losses.

The efficiency of the proposed algorithm was also evaluated using two widely used indicators in the literature—the *SSR* and *SCR*. These indicators were compared for both inverter operation modes over the same days using identical data. Therefore, in both operation modes, the values of these indicators depended solely on changes in imported (or exported) electricity. When imports and exports decreased, these indicators increased, meaning that solar-generated energy was utilized more efficiently. During the study period, the average *SCR* value for the conventional symmetric mode inverter was approximately 19.2%, whereas for the asymmetric mode inverter using the proposed algorithm, it increased to about 24.2%. Similarly, the *SSR* values increased on average from 58.6% to 69.5%.

The AFPM algorithm itself is not complex; however, modeling and analyzing it involved processing vast amounts of data. As mentioned earlier, real-time data from smart meters were transmitted to an SQL server every second, with processing performed later. A total of 518,400 s-by-second power readings were recorded on the server over a 24 h period, with six power values measured per second. Over a month, the total number of recorded power readings exceeded 15.5 million. Measurements were conducted during the spring, summer, and autumn months. Due to various unforeseen circumstances, not all data from this period were fully collected, resulting in a loss of approximately 10% of the data. All collected data were processed, and their daily power profiles were analyzed. In this paper, to explain the operation and characteristics of the proposed algorithm, power profiles for only two days are presented: the "worst" day (with low solar generation) and the "best" day (with relatively high solar generation). For a complete analysis, data from 11 different representative days covering all investigated months were selected and included in the tables.

The APFM algorithm responds to changes in electricity flows within the household grid with a solar power plant and performs balancing within one second. If there are multiple loads with significant power fluctuations within a one-second interval, the algorithm may introduce some error. However, this limitation is not methodological, as it could be addressed by monitoring grid power flows over a shorter time interval and generating control signals for the asymmetric inverter at a higher frequency—something that modern electronics can handle with ease. The potential issue could arise from the inverter's response time to such control signals, but this requires a separate investigation.

When assessing the proposed algorithm's efficiency, all performance indicators in this study were calculated over a 24 h period, meaning they were averaged across the entire day. As a result, the efficiency metrics appear lower compared to when solar generation is active and the AFPM algorithm is in operation. Efficiency could be further improved by integrating energy storage systems that capture excess solar energy and release it when generation ceases. This approach would extend the AFPM algorithm's operational period throughout the day. Future research is planned in this direction. Additional studies will focus on the hardware implementation of the AFPM algorithm. This active power flow management algorithm for household three-phase lines could be integrated into hybrid solar inverters with a neutral wire.

## 6. Conclusions

The research results show that simultaneous active power import and export flows in a three-phase prosumer household grid can be eliminated by employing a proposed active

power flow management (APFM) algorithm. Additionally, the APFM algorithm ensures more symmetrical power export from the household to the DSO grid across all phase lines.

Employing the solar inverter with a neutral wire aided by the APFM algorithm within the household grid results in more efficient use of solar energy generated on-site, minimizing energy exchange with the distribution grid, reducing and balancing the grid load, and improving grid capacity. The simulation of power flows in the household grid of the selected prosumers demonstrated that, on average, daily imported energy from the DSO grid decreased by 27.5%, and exported energy dropped correspondingly. Simultaneously, the relative parameter ($RP_{IMB}$), representing phase line imbalance, declined by an average factor of 5.8.

The same simulation revealed that the APFM algorithm consistently improved the self-consumption rate (*SCR*), a measure of on-site consumption efficiency, across various consumption and generation profiles. The average daily increase was approximately 5%, while a maximum *SCR* increase of 16.6% was observed during periods of lower photovoltaic generation compared to household consumption. The simulation also indicated that as photovoltaic generation rises, the efficiency of on-site consumption decreases (resulting in a lower *SCR*) due to surplus energy being exported.

The self-sufficiency rate (*SSR*), which indicates the portion of self-generated energy in total consumption, improved by an average of 11% while employing the APFM algorithm.

**Author Contributions:** Conceptualization, L.Š., M.V., A.B. and G.S.; methodology, L.Š., M.V., A.B. and G.S.; software, L.Š., J.D. and D.S.; validation, L.Š. and A.B.; formal analysis, L.Š., M.V. and A.B.; investigation, L.Š. and J.D.; resources, A.B.; data curation, L.Š., M.V., A.B. and G.S.; writing—original draft preparation, L.Š., M.V., A.B. and A.K.; writing—review and editing, L.Š., M.V., A.B., G.S., A.K. and A.J.; visualization, L.Š. and J.D.; supervision, M.V., A.B. and G.S.; project administration, S.G.; funding acquisition, S.G. and A.J. All authors have read and agreed to the published version of the manuscript.

**Funding:** This research was funded by the "New Generation Lithuania" (NKL) plan, financed by the European Union's Economic Recovery and Resilience Facility (RRF) as part of the execution of the "Mission-driven Implementation of Science and Innovation Programmes" project (No. 02-002-P-0001) and by the "Technology and Physics Science Excellence Center" (TiFEC) No.S-A-UEI-23-1, financed by the Research Council of Lithuania and the "Misijų projektas".

**Institutional Review Board Statement:** Not applicable.

**Informed Consent Statement:** Not applicable.

**Data Availability Statement:** The data presented in this study are available on request from the corresponding author due to restrictions related to the privacy of private household owners.

**Conflicts of Interest:** The authors declare no conflicts of interest.

## References

1. Kharrazi, A.; Sreeram, V.; Mishra, Y. Assessment Techniques of the Impact of Grid-Tied Rooftop Photovoltaic Generation on the Power Quality of Low Voltage Distribution Network—A Review. *Renew. Sustain. Energy Rev.* **2020**, *120*, 109643. [CrossRef]
2. Madjovski, D.; Dumancic, I.; Tranchita, C. Dynamic Modeling of Distribution Power Systems with Renewable Generation for Stability Analysis. *Energies* **2024**, *17*, 5178. [CrossRef]
3. Sharma, V.; Aziz, S.M.; Haque, M.H.; Kauschke, T. Effects of High Solar Photovoltaic Penetration on Distribution Feeders and the Economic Impact. *Renew. Sustain. Energy Rev.* **2020**, *131*, 110021. [CrossRef]
4. Peprah, F.; Gyamfi, S.; Amo-Boateng, M.; Effah-Donyina, E. Impact Assessment of Grid Tied Rooftop PV Systems on LV Distribution Network. *Sci. Afr.* **2022**, *16*, e01172. [CrossRef]
5. Barutcu, I.C.; Karatepe, E.; Boztepe, M. Impact of Harmonic Limits on PV Penetration Levels in Unbalanced Distribution Networks Considering Load and Irradiance Uncertainty. *Int. J. Electr. Power Energy Syst.* **2020**, *118*, 105780. [CrossRef]

6. Uzum, B.; Onen, A.; Hasanien, H.M.; Muyeen, S.M. Rooftop Solar PV Penetration Impacts on Distribution Network and Further Growth Factors—A Comprehensive Review. *Electronics* **2021**, *10*, 55. [CrossRef]
7. Bandara, C.W.G.; Godaliyadda, G.M.R.I.; Ekanayake, M.P.B.; Ekanayake, J.B. Coordinated Photovoltaic Re-Phasing: A Novel Method to Maximize Renewable Energy Integration in Low Voltage Networks by Mitigating Network Unbalances. *Appl. Energy* **2020**, *280*, 116022. [CrossRef]
8. Pinthurat, W.; Hredzak, B. Dynamic Power Balancing Algorithm for Single-Phase Energy Storage Systems in LV Distribution Network with Unbalanced PV Systems Distribution. *arXiv* **2020**, arXiv:2011.06181. [CrossRef]
9. Wajahat, M.; Khalid, H.A.; Bhutto, G.M.; Leth Bak, C. A Comparative Study into Enhancing the PV Penetration Limit of a LV CIGRE Residential Network with Distributed Grid-Tied Single-Phase PV Systems. *Energies* **2019**, *12*, 2964. [CrossRef]
10. Girigoudar, K.; Roald, L.A. On the Impact of Different Voltage Unbalance Metrics in Distribution System Optimization. *Electr. Power Syst. Res.* **2020**, *189*, 106656. [CrossRef]
11. Pinthurat, W.; Hredzak, B.; Konstantinou, K.; Fletcher, J. Techniques for Compensation of Unbalanced Conditions in LV Distribution Networks with Integrated Renewable Generation: An Overview. *Electr. Power Syst. Res.* **2023**, *214*, 108932. [CrossRef]
12. Suchithra, J.; Rajabi, A.; Robinson, D.A. Enhancing PV Hosting Capacity of Electricity Distribution Networks Using Deep Reinforcement Learning-Based Coordinated Voltage Control. *Energies* **2024**, *17*, 5037. [CrossRef]
13. Mulenga, E.; Bollen, M.H.J.; Etherden, N. A Review of Hosting Capacity Quantification Methods for Photovoltaics in Low-Voltage Distribution Grids. *Int. J. Electr. Power Energy Syst.* **2020**, *115*, 105445. [CrossRef]
14. Gandhi, O.; Kumar, D.S.; Rodríguez-Gallegos, C.D.; Srinivasan, D. Review of Power System Impacts at High PV Penetration Part I: Factors Limiting PV Penetration. *Sol. Energy* **2020**, *210*, 181–201. [CrossRef]
15. Rana, M.M.; Uddin, M.; Sarkar, M.R.; Shafiullah, G.M.; Mo, H.; Atef, M. A Review on Hybrid Photovoltaic—Battery Energy Storage System: Current Status, Challenges, and Future Directions. *J. Energy Storage* **2022**, *51*, 104597. [CrossRef]
16. Kermani, A.; Jamshidi, A.M.; Mahdavi, Z.; Dashtaki, A.; Zand, M.; Nasab, M.A.; Samavat, T.; Sanjeevikumar, P.; Khan, B. Energy Management System for Smart Grid in the Presence of Energy Storage and Photovoltaic Systems. *Int. J. Photoenergy* **2023**, *2023*, 5749756. [CrossRef]
17. Kelm, P.; Mieński, R.; Wasiak, I. Modular PV System for Applications in Prosumer Installations with Uncontrolled, Unbalanced and Non-Linear Loads. *Energies* **2024**, *17*, 1594. [CrossRef]
18. Pinthurat, W.; Hredzak, B. Strategy for Compensation of Unbalanced Powers in LV Residential Distribution Networks Using Distributed Single-Phase Battery Systems. *Electr. Power Syst. Res.* **2022**, *211*, 108253. [CrossRef]
19. Gonzalez-Romera, E.; Ruiz-Cortes, M.; Milanés-Montero, M.I.; Barrero-Gonzalez, F.; Romero-Cadaval, E.; Lopes, R.A.; Martins, J. Advantages of Minimizing Energy Exchange instead of Energy Cost in Prosumer Microgrids. *Energies* **2019**, *12*, 719. [CrossRef]
20. Hokmabad, H.N.; Husev, O.; Kurnitski, J.; Belikov, J. Optimizing Size and Economic Feasibility Assessment of Photovoltaic and Energy Storage Setup in Residential Applications. *Sustain. Energy Grids Netw.* **2024**, *38*, 101385. [CrossRef]
21. Alıç, O. A Holistic Techno-Economic Feasibility Analysis of Residential Renewable Energy Systems: An Insight into Turkish Case. *J. Energy Storage* **2024**, *94*, 112433. [CrossRef]
22. O'Reilly, R.; Cohen, J.; Reichl, J. Achievable Load Shifting Potentials for the European Residential Sector from 2022–2050. *Renew. Sustain. Energy Rev.* **2024**, *189*, 113959. [CrossRef]
23. Brännlund, R.; Vesterberg, M. Peak and Off-Peak Demand for Electricity: Is There a Potential for Load Shifting? *Energy Econ.* **2021**, *102*, 105466. [CrossRef]
24. Griego, D.; Schopfer, S.; Henze, G.; Fleisch, E.; Tiefenbeck, V. Aggregation Effects for Microgrid Communities at Varying Sizes and Prosumer-Consumer Ratios. *Energy Procedia* **2019**, *159*, 346–351. [CrossRef]
25. Cerna, F.V.; Pourakbari-Kasmaei, M.; Pinheiro, S.; Naderi, E.; Lehtonen, M.; Contreras, J. Intelligent Energy Management in a Prosumer Community Considering the Load Factor Enhancement. *Energies* **2021**, *14*, 3624. [CrossRef]
26. Barone, G.; Buonomano, A.; Forzano, C.; Palombo, A.; Russo, G. The Role of Energy Communities in Electricity Grid Balancing: A Flexible Tool for Smart Grid Power Distribution Optimization. *Renew. Sustain. Energy Rev.* **2023**, *187*, 113742. [CrossRef]
27. Pires, V.F.; Cordeiro, A.; Foito, D.; Pires, A.J.; Chen, H.; Martins, J.F.; Castro, R. A Cascaded Dual Four-Leg Inverter for Photovoltaic Systems with Capability to Compensate Unbalanced Distribution Networks. *IEEE J. Emerg. Sel. Top. Ind. Electron.* **2023**, *4*, 960–968. [CrossRef]
28. Alabri, W.; Jayaweera, D. Voltage Regulation in Unbalanced Power Distribution Systems with Residential PV Systems. *Int. J. Electr. Power Energy Syst.* **2021**, *131*, 107036. [CrossRef]
29. Yazdani, S.; Ferdowsi, M.; Davari, M.; Shamsi, P. Advanced Current-Limiting and Power-Sharing Control in a PV-Based Grid-Forming Inverter under Unbalanced Grid Conditions. *IEEE J. Emerg. Sel. Top. Power Electron.* **2020**, *8*, 1084–1096. [CrossRef]
30. Mieński, R.; Wasiak, I.; Kelm, P. Integration of PV Sources in Prosumer Installations Eliminating Their Negative Impact on the Supplying Grid and Optimizing the Microgrid Operation. *Energies* **2023**, *16*, 3479. [CrossRef]
31. Muiste, S.; Pihlap, H.; Tooming, A.; Allik, A. Compensation of Disbalanced Energy Consumption in 3-Phase Systems with Asymmetrical Solar Inverter Output. *Int. J. Renew. Energy Res.* **2021**, *11*, 890–898. [CrossRef]

32. Sriupsa, L.; Vaitkunas, M.; Baronas, A.; Dosinas, J. Analysis of Self-Generated PV Energy Consumption Profiles in Prosumers Microgrid. *Int. J. Sustain. Energy* **2023**, *42*, 1583–1602. [CrossRef]
33. Sriupsa, L.; Dosinas, J.; Vaitkunas, M.; Jonaitis, A.; Baronas, A.; Gudziute, S. Employment of a DC Microgrid for More Efficient Use of Solar Energy in Household Buildings. In Proceedings of the 2022 IEEE 63th International Scientific Conference on Power and Electrical Engineering of Riga Technical University (RTUCON), Riga, Latvia, 10 October 2022; pp. 1–5. [CrossRef]
34. Sungrow Power Supply Co. SG5.0/6.0/7.0/8.0/10/12RT Multi-MPPT String Inverter for 1000 Vdc System. Available online: https://info-support.sungrowpower.com/application/pdf/2023/03/15/DS_20230228_SG5.0_6.0_7.0_8.0_10_12RT_Datasheet_V18_EN.pdf (accessed on 7 January 2025).
35. Fronius Solar Energy. Fronius Symo 3.0-3-M. Available online: https://www.fronius.com/en/solar-energy/installers-partners/products/all-products/inverters/fronius-symo/fronius-symo-3-0-3-m (accessed on 7 January 2025).
36. SOLAR. HUAWEI.COM. Smart String Inverter SUN2000-12/15/17/20KTL-M0. Technical Specification. Available online: https://solar.huawei.com/en-GB/download?p=/-/media/Solar/attachment/pdf/la/datasheet/SUN2000-12-20KTL-M0.pdf (accessed on 7 January 2025).
37. Growatt New Energy CO. WIT 4-15K-HU. Available online: https://en.growatt.com/upload/file/WIT_4-15K-HU_Datasheet_EN_202412.pdf (accessed on 7 January 2025).
38. Smart Meter | Smart Meter | Growatt. Available online: https://en.growatt.com/products/smart-meter (accessed on 7 January 2025).
39. DTSU666-H 100A | Smart Power Sensor-PV Energy Meter | Huawei FusionSolar. Available online: https://solar.huawei.com/en/professionals/all-products/DTSU666-H-100A (accessed on 7 January 2025).
40. Hernández, J.C.; Sanchez-Sutil, F.; Muñoz-Rodríguez, F.J. Design Criteria for the Optimal Sizing of a Hybrid Energy Storage System in PV Household-Prosumers to Maximize Self-Consumption and Self-Sufficiency. *Energy* **2019**, *186*, 115827. [CrossRef]
41. Sudta, P.; Singh, J.G. An Approach to Prosumer Modeling and Financial Assessment with Load Clustering Algorithm in an Active Power Distribution Network. *Sustain. Energy Grids Netw.* **2023**, *38*, 101249. [CrossRef]